

This is an Open Access document downloaded from ORCA, Cardiff University's institutional repository: <https://orca.cardiff.ac.uk/id/eprint/92443/>

This is the author's version of a work that was submitted to / accepted for publication.

Citation for final published version:

Maier, Wolfgang D. , Karykowski, Bartosz and Yang, Shanghong 2016. Formation of transgressive anorthosite seams in the Bushveld Complex via tectonically induced mobilisation of plagioclase-rich crystal mushes. *Geoscience Frontiers* 7 (6) , pp. 875-889. 10.1016/j.gsf.2016.06.005

Publishers page: <http://dx.doi.org/10.1016/j.gsf.2016.06.005>

Please note:

Changes made as a result of publishing processes such as copy-editing, formatting and page numbers may not be reflected in this version. For the definitive version of this publication, please refer to the published source. You are advised to consult the publisher's version if you wish to cite this paper.

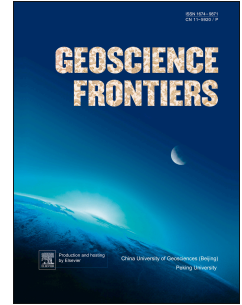
This version is being made available in accordance with publisher policies. See <http://orca.cf.ac.uk/policies.html> for usage policies. Copyright and moral rights for publications made available in ORCA are retained by the copyright holders.



# Accepted Manuscript

Formation of transgressive anorthosite seams in the Bushveld Complex via tectonically induced mobilisation of plagioclase-rich crystal mushes

Wolfgang D. Maier, B.T. Karykowski, Shanghong Yang



PII: S1674-9871(16)30061-5

DOI: [10.1016/j.gsf.2016.06.005](https://doi.org/10.1016/j.gsf.2016.06.005)

Reference: GSF 466

To appear in: *Geoscience Frontiers*

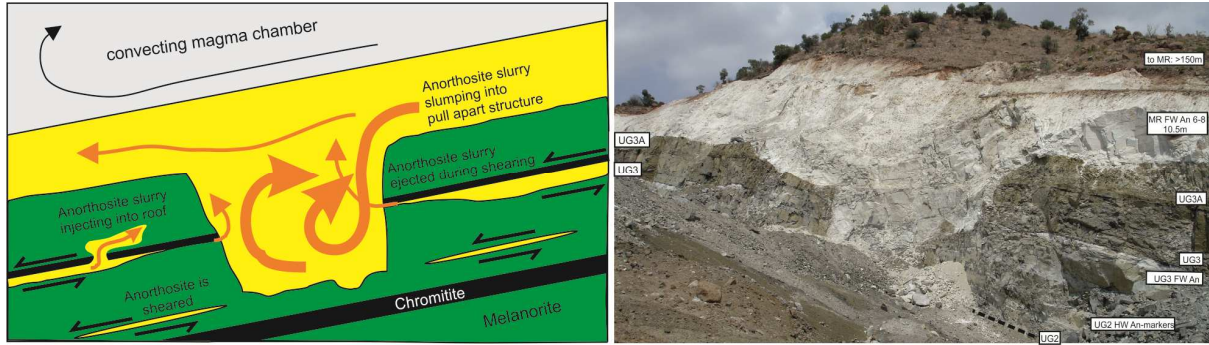
Received Date: 28 March 2016

Revised Date: 14 June 2016

Accepted Date: 17 June 2016

Please cite this article as: Maier, W.D., Karykowski, B.T., Yang, S., Formation of transgressive anorthosite seams in the Bushveld Complex via tectonically induced mobilisation of plagioclase-rich crystal mushes, *Geoscience Frontiers* (2016), doi: 10.1016/j.gsf.2016.06.005.

This is a PDF file of an unedited manuscript that has been accepted for publication. As a service to our customers we are providing this early version of the manuscript. The manuscript will undergo copyediting, typesetting, and review of the resulting proof before it is published in its final form. Please note that during the production process errors may be discovered which could affect the content, and all legal disclaimers that apply to the journal pertain.



# 1 **Formation of transgressive anorthosite seams in the Bushveld Complex via** 2 **tectonically induced mobilisation of plagioclase-rich crystal mushes**

3

4 Wolfgang D. Maier<sup>a,\*</sup>, B.T. Karykowski<sup>a</sup>, Shanghong Yang<sup>b</sup>5 <sup>a</sup> School of Earth and Ocean Sciences, Cardiff University, UK6 <sup>b</sup> Oulu Mining School, University of Oulu, Finland

7 \* Corresponding author e-mail address: maierw@cardiff.ac.uk

## 8 **Abstract**

9 The formation of anorthosites in layered intrusions has remained one of petrology's most  
10 enduring enigmas. We have studied a sequence of layered chromitite, pyroxenite, norite and  
11 anorthosite overlying the UG2 chromitite in the Upper Critical Zone of the eastern Bushveld  
12 Complex at the Smokey Hills platinum mine. Layers show very strong medium to large scale  
13 lateral continuity, but abundant small scale irregularities and transgressive relationships.  
14 Particularly notable are irregular masses and seams of anorthosite that have intrusive  
15 relationships to their host rocks. An anorthosite layer locally transgresses several 10 s of  
16 meters into its footwall, forming what is referred to as a "pothole" in the Bushveld Complex.  
17 It is proposed that the anorthosites formed from plagioclase-rich crystal mushes that  
18 originally accumulated at or near the top of the cumulate pile. The slurries were mobilised  
19 during tectonism induced by chamber subsidence, a model that bears some similarity to that  
20 generally proposed for oceanic mass flows. The anorthosite slurries locally collapsed into  
21 pull-apart structures and injected their hostrocks. The final step was down-dip drainage of Fe-  
22 rich intercumulus liquid, leaving behind anorthosite adcumulates.

23 Keywords: Anorthosite, Layered intrusion, Bushveld Complex, South Africa, Chromitite

## 24 **1. Introduction**

25 The petrogenesis of anorthosites has remained one of petrology's most controversial topics.  
26 Perhaps the key question is how to form a near-monomineralic plagioclase rock from basaltic  
27 magma that crystallises, during most stages of its fractionation, along cotectics and eutectics.  
28 Models advanced in the past include flotation of relatively light plagioclase (Kushiro, 1980),  
29 expulsion of buoyant or dense residual liquid during crystallisation (Morse, 1986; Scoates et

30 al., 2010), oscillating supersaturation of pyroxene and plagioclase (Maaløe, 1978; Morse,  
31 1979a,b), shifting of phase boundaries due to pressure changes in the magma (Naslund and  
32 McBirney, 1996), volatile flux through semi-consolidated cumulates (Nicholson and Mathez,  
33 1992), crystallisation from plagioclase saturated melt generated via resorption of suspended  
34 plagioclase (Hess, 1960) and intrusion of plagioclase mushes derived from staging chambers  
35 (Czamanske and Bohlen, 1990). The model of plagioclase flotation, in combination with  
36 subsequent diapiric ascent of plagioclase crystal mushes, has been widely accepted for  
37 massif-type anorthosites (Ashwal, 1990 and references therein), but none of the above models  
38 can readily explain the enormous lateral extent (up to several 10 s of kilometers) and knife  
39 sharp lower and upper contacts of many anorthosite seams in layered intrusions. This has led  
40 some authors to suggest that anorthosite layers formed through sorting of crystal slurries  
41 moving along the side walls and bottom of magma chambers. Irvine et al. (1998) drew  
42 analogies to turbulent density currents, whereas Maier et al. (2013) preferred a less dynamic  
43 model whereby noritic slurries were sorted and unmixed during their sliding and slumping  
44 along the top of the cumulate pile towards the centre of intrusions, triggered by crustal  
45 subsidence and accompanying seismicity. For the formation of anorthosite adcumulates  
46 which constitute a significant proportion of layered anorthosites both models additionally  
47 require drainage of residual liquid (Scoates et al., 2010).

48 In the present paper, we report further on our initial description (Maier et al., 2013) of a large  
49 anorthosite pothole as well as adjacent intrusive anorthosite at Smokey Hills platinum mine  
50 on the farm Maandagshoek in the eastern Bushveld Complex (Fig. 1A). The evidence  
51 presented suggests that these structures formed in response to a combination of crystal sorting  
52 during slumping of noritic slurries, downward transgression of these slurries across largely  
53 consolidated cumulate layers, and intrusion into a partially solidified crystal pile.

## 54 **2. Regional geology and stratigraphy**

55 The farm Maandagshoek is the discovery site of platinum in the Bushveld Complex  
56 (Merensky, 1926). Platinum nuggets were found in a stream running through the centre of the  
57 farm in June 1924, by farm owner AF Lombaard and Hans Merensky, leading shortly  
58 thereafter to the discovery of the Mooihoek pipe to the SE of the farm (Fig. 1B) and, in  
59 September 1924, the Merensky Reef, close to the discovery site of the nuggets (Fig. 1B).  
60 These discoveries ultimately led to the establishment of the multi-billion dollar South African  
61 platinum industry. Smokey Hills mine was initially opened in January 2008 to exploit the



62 UG2 chromitite exposed on 3 hills along the eastern boundary of the farm (Fig. 1B). After a  
63 temporary halt of operations in 2012–2014, African Thunder Platinum reopened the mine in  
64 early 2015.

65 The stratigraphy of the sequence in this area is summarised in Fig. 1C. The UG2 chromitite  
66 is, on average, 80 cm thick and contains around 8 ppm PGE (Gain, 1985; African Thunder  
67 Platinum internal report). It forms the largest PGE resource on Earth and is mined along >200  
68 km of strike in the Bushveld Complex. It is underlain by ~1 m of pegmatoidal pyroxenite and  
69 harzburgite and overlain by several metres of melanorite containing disseminations and  
70 several thin stringers of chromite, the latter termed “leader seams”. Several meters above the  
71 UG2 chromitite (between 1 and 4 m; Gain, 1985; African Thunder Platinum internal report)  
72 occur the so-called UG2 Hanging Wall Marker Layers, consisting of 2 thin seams of  
73 anorthosite. The seams may locally have thin chromitite stringers at their upper contact  
74 (Gain, 1985) and are located in a ~1 m layered noritic interval. Both Marker Layers are also  
75 developed at Atok mine, some 50 km to the NW of Smokey Hills mine and thus appear to be  
76 regionally broadly continuous. Another relatively feldspathic interval, consisting of a ~2 m  
77 norite and melanorite that is banded on a cm scale occurs approximately 5 m above the UG2  
78 chromitite. This interval is overlain by a magmatic breccia, comprising numerous autoliths of  
79 melanorite, pyroxenite and anorthosite in a noritic matrix. Next is a ~60 cm anorthosite layer  
80 that forms the footwall to the UG3 chromitite throughout much of the northeastern Bushveld,  
81 i.e., from Atok to Maandagshoek (Gain, 1982; Mossom, 1986). The overlying ~25 cm thick  
82 UG3 chromitite contains approximately 3 ppm PGE (Gain, 1982), but is generally not mined  
83 in the Bushveld. Next follows approximately 5 m of melanorite that is distinctly more Ni rich  
84 than the UG3 footwall melanorite (Gain, 1985) and that contains low grade PGE  
85 mineralisation throughout (~0.5 ppm; Gain, 1985). Both the UG3 chromitite and hanging  
86 wall melanorite show a pronounced Pt enrichment relative to Pd, matched by few other layers  
87 in the Bushveld Complex.

88 The next prominent layers consist of the UG3a-b doublet, formed by 2 thin chromitites, each  
89 on average 12 cm wide, and located within a 1–2 m sequence of predominantly harzburgite  
90 and pyroxenite (Gain, 1985). This is overlain by a further 5 m of melanorite before the  
91 contact with a thick (up to 350 m), predominantly feldspathic, sequence is reached termed the  
92 Merensky Reef footwall sequence in the Bushveld mines. This is normally sub-divided into 8  
93 units of which the lowermost 3 (units 8–6) are exposed at Smokey Hills mine. The base of the  
94 feldspathic sequence is knife sharp and defined by a 1–2 mm chromitite stringer that

95 undulates vertically on a scale of millimetres to meters, and laterally centimetres to 10 s of  
96 meters. The contact resembles that exposed at the base of the Upper Critical Zone at Cameron  
97 Section, but with mostly longer and less regular wavelengths. The chromitite is overlain by  
98 mottled anorthosite (Merensky Reef footwall 8 and 7). This interval is developed in broadly  
99 similar thickness at Atok mine, some 50 km to the NW and thus appears to be regionally  
100 largely continuous. It is overlain by so-called “spotted anorthosite” (MR footwall 6), a term  
101 used in Bushveld mines denoting a plagioclase-rich rock with up to around 10% cumulus  
102 pyroxene. This in turn grades upwards into norite (MR footwall 5).

### 103 **3. New field observations**

104 The bulk of the studied sequence is exposed on the slopes of Hills 2 and 3 at Smokey Hills  
105 Mine (Fig. 1B), notably in several opencast pits, of which the largest is shown in Fig 2. The  
106 UG2 seam is not accessible in most of the open pits due to their partial refill with waste, but it  
107 is well exposed along the access road to the mine.

#### 108 *3.1 UG2 Chromitite*

109 The UG2 chromitite forms the base of the exposed sequence. The main seam has sharp  
110 bottom and top contacts (Fig. 3A). It is relatively undisturbed over approximately 200 m of  
111 exposure along the road cut; Major potholes are not apparent, which is notable in view of the  
112 abundance of potholes at, e.g., the UG2 exposure at Karee mine described by van der Merwe  
113 and Cawthorn (2005). However, small-scale transgressions into the footwall, somewhat  
114 analogous to those at Karee, are common, although the footwall at Maandagshoek is  
115 pyroxenite as opposed to anorthosite at Karee. Characteristic for UG2 exposures throughout  
116 the eastern Bushveld are numerous autoliths of pyroxenite and, locally, anorthosite and  
117 pegmatoid (Fig. 3). The autoliths are mostly highly elongated, with lengths up to several  
118 meters and thicknesses of mostly less than a few centimeters. They tend to be oriented  
119 parallel to the contacts of the seam. Examination of similar autoliths in 3D outcrop of  
120 chromitite from elsewhere (e.g., the LG6 seam at Cameron Section) suggests that many of the  
121 autoliths are disc shaped. The UG2 seam also contains cm- to dm-sized irregular masses of  
122 anorthosite intruding the chromitite and its hangingwall (Fig. 3B). In places, the upper  
123 portion of the UG2 bifurcates, resulting in a thin chromitite stringer branching off into the  
124 roof. It is our impression that the thin leader seams, located a few centimetres to decimetres  
125 above the main seam, are the result of such bifurcations.

#### 126 *3.2. The UG2 hanging wall marker layers*

127 The marker layers are well exposed in the main pit (30°7'36"E, 24°35'15"S) and a subsidiary  
128 pit approximately 50 m to the N of the main pit. They consist of two laterally relatively  
129 continuous anorthosite seams, 3–30 cm in thickness, as well as numerous highly elongated  
130 schlieren of anorthosite between and, to a lesser extent, below and above the marker layers  
131 (Fig. 4). The layers appear to be nearly pure anorthosite with just a weak concentration of  
132 pyroxene mottles. The layers are hosted within a ~1 m distinctly banded interval of relatively  
133 leucocratic and melanocratic norite. Within the lower anorthosite seam there is a banded  
134 noritic-anorthositic horizon whose upper contact is itself transgressed by anorthosite (Fig.  
135 4B). In several instances, the marker layers form cusps or flames injecting into the hanging  
136 wall (Fig. 4C, D). The cusps are pointing in a broadly northerly direction. The lower contacts  
137 of the marker layers are also irregular, but they are less transgressive than the upper contacts.

### 138 *3.3. The interval between the UG2 hanging wall marker layers and the UG3 chromitite*

139 The interval is approximately 15 m thick. It consists predominantly of melanorite (Gain,  
140 1985), but 2–3 m below the UG3 chromitite is a relatively feldspathic, strongly banded  
141 interval containing decimetre-sized blocky autoliths of anorthosite (Fig. 5A, B). It is overlain  
142 by a poorly layered magmatic breccia consisting of similar anorthosite fragments as  
143 mentioned above, but hosted in larger melanocratic fragments that are distributed within a  
144 relatively leucocratic matrix (Fig. 5A). This breccia is also exposed in a stream gully,  
145 approximately 1 km to the S of the mine. The breccia is overlain by the UG3 footwall  
146 anorthosite (Fig. 5A). This consists of 3 distinct horizons, namely an upper mottled portion, a  
147 central banded portion, and a lower schlieren-banded portion (Fig. 5C, D). The anorthosite  
148 locally wedges out (Fig. 5A), notably near both edges of the large anorthosite pothole (Figs.  
149 2, 5A), and towards the N of the pit. The lower and upper contacts of the anorthosite are  
150 seemingly intrusive into the footwall norite and the hanging wall UG3 chromitite (Fig. 5C).

### 151 *3.4. The UG3 Chromitite*

152 The seam can be traced around most of hills 2 and 3 (Fig. 1). The relationship between the  
153 chromitite and its footwall anorthosite is complex. The chromitite may locally contain  
154 autoliths of anorthosite, but is elsewhere injected by rounded and flame-like protrusions of  
155 anorthosite (Fig. 5C). Above this injection the chromitite and its immediate hanging wall are  
156 slightly domed up, but the rocks approximately 1 m above the injection have a horizontal  
157 configuration. In a subsidiary pit to the S of the main pit, anorthosite forms a large irregular  
158 pod-like mass, brecciating the UG3 chromitite and its pyroxenitic and melanoritic host rocks



159 (Fig. 6). The UG3 chromitite is additionally intruded by pyroxenite at this locality (Fig. 6C).  
160 Notably, the UG3 chromitite does not appear to form significant potholes in the open pits, but  
161 in the stream gully to the S of the mine the footwall anorthosite has been potholed  
162 extensively by pyroxenite with only thin basal coronas of chromitite exposed, possibly  
163 suggesting that the UG3 hanging wall pyroxenite potholed both the chromitite and its  
164 anorthositic footwall. In yet another variety of potholing, at Atok mine, both the UG3 and its  
165 footwall anorthosite may together pothole the underlying noritic rocks (Mossom, 1986).

166 The UG3a and b could not be studied in detail due to lack of accessible exposure. The  
167 uppermost chromitite of the sequence is represented by the thin but persistent stringer at the  
168 upper contact of the UG3 hanging wall melanorite with the Merensky Reef footwall 7–8  
169 anorthosite (Fig. 7D).

### 170 *3.5 The Merensky Reef footwall units 7-8 (FW 7-8)*

171 Footwall 8 consists of a basal mottled anorthosite interlayered with spotted anorthosite.  
172 Footwall 7 is mottled anorthosite, grading upwards into spotted anorthosite and leuconorite of  
173 Footwall 6 and then norite (FW5). The mottled anorthosite has a heterogenous texture,  
174 containing noritic bands as well as mottled portions showing highly variable density and size  
175 of mottles (Fig. 7E). Along the length of the exposure at Smokey Hills mine, the anorthosite  
176 contains numerous bodies of pyroxenite and melanorite. Some of these bodies are pipe-like  
177 and likely represent members of the IRUP family (iron-rich ultramafic pipes), but banded  
178 melanorite possibly representing autoliths of the underlying units also occur (Fig. 7A).

179 On Hill 3 the Merensky Reef footwall 8-6 anorthosite forms a large transgressive pothole,  
180 approximately 20 m deep (Fig. 2). The lower trough of the pothole is 10–20 m wide, but the  
181 upper portion of the pothole is up to ~40 m wide. The anorthosite in the pothole shows a faint  
182 trough banding (Fig. 7B). The sidewalls of the lower trough are sub-vertical (Fig. 2) which  
183 suggests that brittle deformation played a role in its formation. However, the sequence on  
184 both sides of the pothole is at a broadly similar stratigraphic position, ruling out significant  
185 downward faulting associated with the pothole. The wall of the upper trough has a much  
186 shallower slope than that of the lower trough (Fig. 2). Along the southern sidewall, 2 thin  
187 slivers of mafic material, possibly iron-rich ultramafic rock, extend for several m into the  
188 pothole (Figs. 2 and 7C). In places, large blocks of the sidewall, consisting of UG3 chromitite  
189 and its hanging wall pyroxenite have been partially dislodged and are engulfed in anorthosite  
190 (Fig. 8). Along the northern sidewall the transgressive anorthosite appears to inject the side

191 wall above and below the consolidated UG3 pyroxenite package (Fig. 8B). The bottom  
192 contact of the pothole is also highly irregular.

### 193 *3.6. Iron rich ultramafic pipes (IRUP)*

194 IRUPs are well exposed, e.g., in the southern subsidiary pit where they occur within the UG3  
195 footwall and hanging wall sequence, and in the NE face of hill 2 where they form irregular  
196 sub-vertical bodies within the Merensky Reef FW anorthosite (Fig. 7A). They can be several  
197 meters wide and mostly have sharp basal terminations, either within or at the basal contact of  
198 the host anorthosite. In one instance, the IRUP terminates on top of a melanorite autolith (Fig.  
199 7A).

## 200 **4. Petrography and mineral compositional data**

201 In order to gain an improved understanding of the origin of the anorthosite we have analysed  
202 four samples, one each from the large anorthosite pothole, the UG3 footwall anorthosite, the  
203 Merensky Reef FW 8 mottled anorthosite and the Merensky Reef FW7 spotted anorthosite.

204 Sample 1 comprises a norite band in anorthosite, located approximately 1 m above the base  
205 of the large anorthosite pothole exposed in the main pit (see Fig. 2 for sample position, GPS  
206 30°7'36"E, 24°35'15"S). The anorthosite is an adcumulate and has a sharp and undulating  
207 contact to the norite band. Plagioclase grains in the anorthosite reach 3–4 mm in size (but are  
208 mostly < 1 mm long), showing serrated and highly irregular grain boundaries (Fig. 9A)  
209 indicative of late magmatic or post magmatic deformation. Other evidence for deformation  
210 includes abundant undulous extinction and annealing of grains to form complex larger grains.  
211 The norite is medium grained and contains approximately 60% subhedral orthopyroxene  
212 (mostly 0.5–1 mm wide) and 40% subhedral plagioclase of broadly similar grain size (Fig.  
213 9B). Plagioclase is preferentially concentrated in mm-wide stringers oriented sub-parallel to  
214 the contact between anorthosite and norite (Fig. 10).

215 Sample 2 comprises a 1 cm wide band of norite in anorthosite, located ~30 cm below the  
216 UG3 chromitite. It was collected in a subsidiary pit 200 m to the S of the large pothole (GPS  
217 30°7'40"E, 24°35'21"S). The norite band is approximately 1 cm thick and bounded in its  
218 footwall and hanging wall by a 0.5–1 cm wide anorthosite adcumulate (Electronic Appendix  
219 1). The hanging wall anorthosite adcumulate is overlain by faintly banded anorthosite-  
220 leuconorite that may contain large (up to 1 cm) clinopyroxene oikocrysts which are slightly  
221 elongated parallel to the layering. Plagioclase in the HW anorthosite adcumulate is typically

222 around 2–3 mm long, strongly foliated and almost as deformed as in the anorthosite of  
223 sample 1, but it lacks composite recrystallized grains (Fig. 9C). Orthopyroxene in the  
224 anorthosite is relatively large (up to about 3 mm), anhedral, and contains numerous sub-  
225 rounded plagioclase inclusions that appear to be less deformed than the cumulus plagioclase  
226 in norite and anorthosite, as judged by their relatively straight twin lamellae. Plagioclase in  
227 the norite band is mostly < 1 mm wide and has abundant spindle-shaped twin lamellae.  
228 Orthopyroxene in the norite band is subhedral and measures around 1 mm in width and  
229 length (Fig. 9D). In both norite and anorthosite, plagioclase is distinctly reverse zoned  
230 (Electronic Appendix 2), analogous to the results of Maier and Eales (1997) from the  
231 Merensky Reef-UG2 interval in the western Bushveld Complex (Electronic Appendix 3)  
232 which revealed reverse zoning towards slightly higher An (< 3–4 % An) in 9 of 10 cumulus  
233 plagioclase grains and 16 of 20 plagioclase inclusions in orthopyroxene. In sharp contrast to  
234 these Bushveld plagioclase grains, plagioclase in noritic and anorthositic cumulates of other  
235 layered intrusions, e.g., Rum, may show pronounced normal zoning with variations  
236 commonly around 20% An content (O’Driscoll et al., 2009).

237 Sample 3 is a mottled anorthosite collected approximately 2 m above the base of the  
238 Merensky Reef FW 8 anorthosite, in the same pit as sample 2. It is strongly foliated and most  
239 plagioclase grains are relatively large, typically up to around 3 mm (locally up to 5 mm) (Fig.  
240 9E). However, plagioclase grain size is much reduced in certain 1–2 mm wide patches  
241 characterised by the presence of intercumulus pyroxene and enhanced alteration. Optical  
242 microscopy indicates a broadly similar degree of zoning as in samples 1 and 2. Although  
243 there are some spindle shaped twin lamellae and indented grain boundaries, the degree of  
244 deformation is much less than in samples 1 and 2. Many grain boundaries are approaching  
245 120°. As in sample 2, plagioclase inclusions in orthopyroxene oikocrysts are notably less  
246 deformed than those outside the oikocrysts.

247 Sample 4 is a spotted anorthosite from the Merensky Reef FW 7, collected approximately 3  
248 m above the base of the MR FW 8, in a further subsidiary pit located between sample locality  
249 1 and 2–3. Plagioclase grains are mostly between 1 and 2 mm long (locally up to 5 mm).  
250 Foliation and deformation are moderate, i.e., few of the twin lamellae are bent, and the grains  
251 show relatively little undulous extinction. The rock contains small (<1 mm) anhedral and  
252 subhedral orthopyroxenes (Fig. 9F) and large oikocrysts of clinopyroxene.

253 Mineral compositions have been determined for samples 1 and 2 (Electronic Appendix 4).  
254 Anorthosite in sample 1 has slightly lower An contents than norite (73.4 vs 74.5) and Mg<sup>#</sup> of  
255 orthopyroxene is also slightly lower (78.9 vs 80.2). No zonation is apparent using optical  
256 microscopy or SEM. In sample 2, mean anorthite content of plagioclase in norite is 76.8,  
257 slightly higher than in sample 1, whereas Mg<sup>#</sup> of orthopyroxene is 79.9, similar to sample 1.  
258 In general, plagioclase has very similar compositions as in norite and anorthosite of the UG2-  
259 Merensky Reef interval in the western Bushveld Complex (Maier and Eales, 1997). We  
260 cannot confirm the findings of Gain (1985) who reported strongly elevated anorthosite  
261 content (>83%) in plagioclase within the UG3 footwall anorthosite. Our anorthosite contents  
262 (and Mg<sup>#</sup> of opx) are, however, broadly similar to those of Mondal and Mathez (2007) who  
263 found An values between 70 and 75% and Mg<sup>#</sup> of orthopyroxene around 80 in the interval  
264 between the UG2 and UG3 chromitites. A further notable result of the element mapping of  
265 samples 1 and 2 is the lack of An contents below 60 and Mg<sup>#</sup> below 75, suggesting very  
266 effective draining of the most differentiated residual liquids. It is presently not known to what  
267 degree this feature is unique to the Upper Critical Zone, or the Bushveld Complex as a whole.

268 In the present study, we did not determine whole rock compositions of our samples. The data  
269 of Maier and Eales (1997) indicate that UCZ anorthosite and norite has very low  
270 incompatible trace element contents, e.g., an average of 3.9 ppm Zr in 25 samples, suggesting  
271 <5% trapped liquid component. This is consistent with very effective removal of  
272 intercumulus liquid, or adcumulus growth at the top of the crystal pile.

## 273 **5. Summary and interpretation of key observations**

274 (1) The ~20 m interval between the UG2 chromitite and the Merensky Reef footwall 7-8  
275 anorthosite in the eastern Bushveld Complex is prominently layered, with individual units  
276 displaying well developed lateral continuity on a scale of kilometers to 10s of km. However,  
277 exposure of the sequence at Smokey Hills mine on the farm Maandagshoek indicates that on  
278 a scale of centimetres to meters lateral continuity is poor, showing strong thickness variation,  
279 abundant transgressive relationships between layers, and numerous intrusive bodies of  
280 anorthosite and ultramafic rock (Figs. 3–8). Following Maier et al. (2013) and Forien et al.  
281 (2016) we interpret the broader scale layering to have formed through hydrodynamic sorting  
282 and kinetic sieving of crystal slurries. The main arguments are of structural and  
283 compositional nature; First, the abundant slumping- and syn-magmatic deformation structures  
284 in the Upper Critical Zone show strong similarities to those in oceanic mass flows interpreted

285 to have been deposited from liquefied sediments surging down sloped continental shelves.  
286 Second, the enrichment of PGE and sulphides at the ultramafic base rather than the mafic top  
287 of cyclic units is inconsistent with the strongly S undersaturated nature of Bushveld parent  
288 magmas (c.f., Barnes et al., 2010) and is more readily explained by efficient redistribution of  
289 sulphides that originally accumulated in the more fractionated portions of units. Based on  
290 intrusive relationships of certain ultramafic layers with regard to their hanging wall, Maier  
291 and Barnes (2008) and Maier et al. (2013) further argued that ultramafic and anorthositic  
292 crystal slurries may locally inject in a sill-like manner into the semi-consolidated cumulate  
293 package while they slide down along the top of the crystal pile.

294 (2) The stratigraphy of the UG2 hanging wall sequence at Smokey Hills mine shows some  
295 important differences to that in the western Bushveld Complex (Maier and Eales 1997); The  
296 ultramafic sequence above the UG2 chromitite is mostly around 10 m thick in the western  
297 Bushveld, whereas it measures around 20 m in the eastern Bushveld. Also, the UG3  
298 chromitite seams are not developed in the west and the UG2 main seam is instead overlain  
299 by several so-called “leader seams” that may have thicknesses of centimeters to decimetres,  
300 show local bifurcation, and may be located up to several meters above the main seam (Leeb-  
301 du Toit, 1986). It is suggested that the UG3 seams at Smokey Hills mine are the stratigraphic  
302 equivalents of the UG2 leader seams in the western Bushveld.

303 (3) In common with many of the most strongly layered intervals of the Bushveld Complex,  
304 the Smokey Hills sequence contains abundant autoliths, notably within the UG2 chromitite  
305 and a noritic interval below the UG3 chromitite that resembles a magmatic breccia (Fig.  
306 5A,B). These observations are consistent with previous studies which proposed that the UG2  
307 unit represents an interval of particularly vigorous magma replenishment (Eales et al., 1986,  
308 1988; Naldrett et al., 1986, 2012; Maier et al., 1994; Maier and Eales, 1997), partially eroding  
309 the top of the cumulate pile. Replenishment of the chamber with fertile magma is also  
310 consistent with the high PGE content of the UG2 unit relative to the underlying units (Gain,  
311 1985).

312 (4) Anorthosite layers at Smokey Hills mine show transgressive and irregular contacts with  
313 both their hanging wall and footwall rocks (Figs. 4–8). We argue that this reflects sill-like  
314 injection of anorthositic magmas into a largely consolidated cumulate package. Unambiguous  
315 anorthosite injection, as well as potholing of pyroxenite and chromitite by anorthosite, is  
316 particularly prominent where the sequence is locally thinned, the latter interpreted to result



317 from down-dip syn-magmatic stretching of the cumulates. In some cases, field observations  
318 such as the flame-like anorthosite tongues in chromitite (Fig. 5C) suggest that both the  
319 anorthosite and its chromitite hanging wall were crystal mushes during injection, but adjacent  
320 to the large pothole seemingly consolidated UG3 chromitite is brecciated by intrusive  
321 anorthosite (Fig. 8). Thus the combined field data suggest that anorthosite and chromitite  
322 layers formed broadly simultaneously.

323 (5) Highly elongated schlieren of anorthosite within the UG2 hanging wall marker horizon  
324 (Fig. 4), noritic schlieren within the UG3 footwall anorthosite (Fig. 5D) and elongated  
325 autoliths of pyroxenite within the UG2 chromitite (Fig. 3) all imply layer-parallel ductile  
326 deformation. Micro textural observations also reveal widespread deformation features  
327 including stringers of plagioclase within norite lenses in pothole anorthosite (Fig. 10),  
328 undulous extinction, sub-grain formation and spindle twins in plagioclase (Fig. 9). The  
329 absence of significant fracturing and hydrothermal alteration suggest that deformation  
330 occurred syn-magmatically, at a relatively high temperature.

331 (6) The present study provides new insight into the origin of potholes. Of particular interest is  
332 the large anorthosite pothole (Fig. 2), considering that anorthosite potholes are relatively rare  
333 in layered intrusions. Eales et al. (1988) have proposed that potholes form through thermo-  
334 chemical-mechanical erosion of footwall cumulates by relatively primitive replenishing  
335 magma. However, formation of the present anorthosite pothole via thermo-chemical erosion  
336 of ultramafic cumulates would require the existence of superheated anorthositic magma,  
337 perhaps formed during depressurisation of ascending feldspathic slurries (Naslund and  
338 McBirney, 1996). We consider this model to be improbable as assimilation of ultramafic  
339 floor cumulates would drive the composition of the magma towards the cotectic with  
340 pyroxene, inconsistent with the development of thin intrusive seams and transgressive cusps  
341 of anorthosite within norite, pyroxenite and chromitite.

342 The anorthosite pothole has sub-vertical sidewalls suggesting that its formation was  
343 structurally controlled. The location of the pothole above a thinned cumulate succession  
344 could suggest that the formation of the pothole is related to stretching of the footwall rocks,  
345 possibly triggered by subsidence of the centre of the intrusion in response to crustal loading  
346 (Maier et al., 2013) locally leading to failure and pull-apart structures into which anorthositic  
347 crystal mushes slumped. The vortex of the slumping magma potentially widened the pothole  
348 and caused undercuts and dismemberment of the sidewalls, particularly at layer contacts. A

349 model of within-layer penetrative strain is consistent with the observed thinning of the  
350 sequence towards the pinch of a pinch and swell structure. In broad terms, the pothole  
351 resembles a boudin gap or pull apart extension progressively filled by relatively less viscous  
352 matrix material. Pull apart structures typically have regular sub-vertical walls, but they may  
353 locally show irregular boudin ends informally called fish mouths, resembling the sidewalls of  
354 the pothole (Fig. 8C). The anorthosite pothole thus presents a rare and unique snapshot of the  
355 early stages of formation of large potholes. Intriguingly, the UG3 footwall anorthosite  
356 pinches out on both sides of the pothole (Fig. 2). Anorthosite tends to be more competent  
357 than mafic rocks (Svahnberg, 2010) and thus the pinching out suggests that the anorthosite in  
358 the seam was incompletely solidified at the time of stretching and pothole formation. This  
359 may have allowed tectonic expulsion of the anorthosite magma. In contrast, the bulk of the  
360 remainder of the sequence was apparently largely solidified, as indicated by the angular  
361 chromitite-pyroxenite autoliths in the pothole.

362 (7) The formation of anorthosite adcumulates, at Smokey Hills mine (Fig. 9A,C,E; Electronic  
363 Appendix 1) and elsewhere, remains enigmatic. Based in part on the trough-like layering in  
364 the pothole anorthosite (Fig. 7B) we argue that the intruding magma was a slurry containing  
365 abundant plagioclase crystals. This model is consistent with many of the macroscopic and  
366 microscopic textures observed (Fig. 9A). Assuming that the cotectic ratio between  
367 plagioclase and pyroxene is approximately 60:40, it can be estimated that a basalt with ~50 %  
368 suspended plagioclase crystals (the maximum crystal content permissible in a flowing mush;  
369 Paterson, 2009) would solidify to have approximately 20% pyroxene. This is clearly in  
370 excess of the pyroxene content of the studied anorthosites which contain mostly < 5%  
371 pyroxene. Thus, either the anorthosites crystallised from a magma containing both a high  
372 crystal load of plagioclase and a liquid component supersaturated in plagioclase, or a large  
373 amount of residual liquid was drained from the plagioclase-rich mush prior to solidification,  
374 possibly in a down-dip direction (Scoates et al., 2010). In the absence of clear evidence for  
375 the presence of plagioclase supersaturated magma, in the Bushveld Complex and elsewhere,  
376 we favour the model of rapid and efficient draining of residual liquid. This model is  
377 consistent with the general paucity in incompatible trace elements in Bushveld anorthosite  
378 (Maier and Eales, 1997) and it shares certain features with that generally favoured for the  
379 formation of anorthosite massifs, namely initial emplacement of crystal slurries, followed by  
380 downward draining of residual liquid (Scoates et al., 2010; Arndt, 2013; Maier et al., 2013).

381 (8) The ubiquitous reverse zonation of plagioclase is perplexing and has been explained by  
382 equilibration of the grains with a late percolating hydrous melt that led to preferential  
383 resorption of albite component (Boudreau, 1988; Maier, 1995). Maier (1995) has shown that  
384 the fluids may be locally concentrated to form phlogopite-rich oikocrysts of olivine and  
385 pyroxene. Whether reversed zonation of plagioclase is unique to the Bushveld Complex, or to  
386 the UG2-Merensky Reef interval, remains presently unclear. In their study of 11 Upper Zone  
387 and Main Zone plagioclase grains, Tanner et al. (2014) found subdued zonation (mostly <4%  
388 An variation across grains), with just 4 of the grains being reversed zoned. The Bushveld  
389 Complex is an order of magnitude larger than other layered intrusions, and thus likely cooled  
390 slower. This could have led to relatively prolonged mobility of late magmatic hydrous fluid,  
391 followed by effective melt drainage in response to chamber subsidence. The effects of  
392 potentially elevated CO<sub>2</sub> in the magma, derived from devolatilisation of the Transvaal  
393 dolomites in the floor of the intrusion also remain poorly studied. The solubility of CO<sub>2</sub> in  
394 basalt is relatively low (up to ~0.2 wt.%; Wallace et al., 2015), so the effect on the T of the  
395 plagioclase solidus would possibly be minor, but the presence of CO<sub>2</sub> bubbles in the flowing  
396 crystal mush could dramatically lower melt viscosity (Leshner and Spera, 2015) thereby  
397 facilitating sorting and compaction of the crystal mush, and residual melt expulsion.

398 (9) Transgressive ultramafic bodies, likely belonging to the ITUP family, are abundant at  
399 Smokey Hills mine and in its vicinity, e.g., at the nearby Mooihoek and Driekop pipes (Scoon  
400 and Mitchell, 2011). The field data suggest an important component of horizontal or  
401 downward movement of the IRUP magma (e.g., Fig. 12 in Maier et al., 2013). It is presently  
402 unclear whether IRUPs are relatively more abundant at Smokey Hills mine and surroundings  
403 than elsewhere in the Bushveld Complex, whether this might reflect the exceptionally good  
404 outcrop conditions in the mine, or whether IRUPs are genetically related to the large  
405 anorthosite pothole. Following Scoon and Mitchell (1994) we propose that the IRUPs  
406 represent the immiscible Fe rich end-member of residual liquids drained from anorthosites,  
407 with the relatively buoyant silica and alkali rich end-member liquid having escaped into the  
408 supernatant magma column. This model is consistent with the close spatial association of  
409 IRUPs and anorthosites on Mandagshoek and elsewhere, namely on the farm Tweefontein,  
410 eastern Bushveld Complex where anorthosite and norite fragments occur within an IRUP  
411 pipe (**Electronic Appendix 5**; Boorman et al., 2003). The latter authors interpreted the pipe  
412 to have formed from upward migrating fluid, but an alternative interpretation is that it

413 represents collapse of an incompletely consolidated norite-anorthosite mush into a pull apart  
414 structure, followed by downward draining of Fe-rich residual liquid.

## 415 **6. Sequence of deformational and intrusive events**

416 Our observations allow us to place some constraints on the sequence of magmatic and  
417 structural events, summarised in Fig. 11. (1) Amongst the earliest events was the hot shearing  
418 leading to the formation of anorthosite schlieren in, e.g., the UG2 hanging wall marker layers,  
419 the noritic schlieren in the UG3 footwall anorthosite and the elongated pyroxenite autoliths in  
420 the UG2 chromitite, which all indicate significant layer-parallel deformation. Whether this  
421 deformation was coeval with, or postdated the formation of the macro layering of the  
422 sequence remains to be determined, e.g., by microtextural analyses using EBSD. (2) Small  
423 anorthosite potholes within norite lenses in the UG2 hanging wall marker interval are little  
424 deformed and thus likely postdated the hot shearing. The same applies to the anorthosite  
425 flames within, and the updoming of, the UG3 chromitite. This suggests that the UG3 footwall  
426 anorthosite and the UG2 hanging wall marker anorthosite layers each consist of several sub-  
427 layers that intruded at a different time. It also implies that anorthosite is one of the last rocks  
428 to solidify in the studied sequence. (3) The large anorthosite pothole formed next, following  
429 the thinning of the sequence below the pothole, related to down-dip stretching of the entire  
430 UG2 unit. (4) The pinching out of the UG3 footwall anorthosite adjacent to the pothole  
431 suggests that the former was still in a mush state when the sequence was stretched and the  
432 pothole formed. We conclude that anorthosite layers served as lubrication planes during  
433 cumulate deformation. We propose that phase sorting during the early stage of layer  
434 formation led to plagioclase rich mushes enriched in relatively light, volatile rich residual  
435 liquid. These mushes were covered by new cumulate layers. Frequent tectonism and  
436 readjustment of the chamber then led to liquefaction, mobilisation and intrusion of  
437 anorthosite mushes into zones of dilation. The paucity of incompatible trace elements in these  
438 rocks indicates very efficient draining of residual liquid prior to final solidification, forming  
439 IRUPs. The shape of the IRUPs indicates that liquid was drained parallel to the layering and  
440 downwards across the layering.

## 441 **7. Analogies between continental and oceanic layered intrusions**

442 Gabbroic intrusions at mid-ocean ridges may be layered at the cm to 10s of cm scale, often  
443 showing well developed density grading within layers but also knife-sharp boundaries  
444 between anorthosite, troctolite and ultramafic layers. Similar to the Bushveld layers, the

445 mineral compositions of the oceanic intrusions show little variation, inconsistent with  
446 fractionation. Instead, the formation of the layers has been interpreted through a combination  
447 of frequent magma replenishment and hot shearing of cumulates (Jousselin et al., 2012),  
448 analogous to the model proposed here for the Bushveld Complex. The main difference  
449 between the continental and oceanic intrusions is that in the latter process was driven by  
450 mantle flow rather than chamber subsidence.

## 451 **8. Conclusions**

452 Our understanding of the petrogenesis of layered intrusions, and the Bushveld Complex in  
453 particular, has made significant advances in the last decade, partly due to new exposures of  
454 the Upper Critical Zone that have become accessible in a number of open pits (e.g., van der  
455 Merwe and Cawthorn, 2005). The open pits at Smokey Hills mine are particularly revealing,  
456 being that they present up to 1 km of continuous lateral exposure of the UG2 hanging wall  
457 sequence. The characterisation and study of these rocks is still in its early stages, but initial  
458 observations allow us to propose the following preliminary petrogenetic model (Fig. 12): (1)  
459 The pronounced layering of the sequence formed largely through hydrodynamic sorting and  
460 kinetic sieving of crystal slurries at the top of the cumulate pile in response to chamber  
461 subsidence. This process resulted in distinct, sharply bound layers of chromitite, melanorite,  
462 and anorthosite and in enrichment of sulphides and PGE at the ultramafic base of units. (2)  
463 Plagioclase-rich layers contained relatively large proportions of buoyant residual liquid and  
464 thus remained incompletely solidified for a relatively long time. (3) The distinct density  
465 contrasts between layers, notably where chromitite overlaid anorthosite led to local flame-like  
466 intrusion of anorthosite mush into, and up-doming of, the hanging wall chromitite,  
467 reminiscent of load cast structures in sedimentary deposits. (4) Continued subsidence of the  
468 central portion of the intrusion in response to crustal loading caused stretching and flexing of  
469 the uppermost portion of the cumulate pile, resulting in pinch-and-swell structures. Semi-  
470 consolidated anorthosite layers located near the top of the crystal pile acted as lubrication  
471 planes facilitating structural failure and opening of pull-apart structures. (5) Hot shearing  
472 within the cumulate pile led to remobilisation of some of the buried anorthosite mushes, and  
473 injection into their footwall and hanging wall. (6) Anorthosite slurries located at the top of the  
474 cumulate pile collapsed into the pull-apart structures leading to the formation of large  
475 anorthosite potholes.



476 Our study concludes that layering in the Bushveld Complex and other mafic-ultramafic  
477 intrusions formed through a combination of magmatic and structural processes. Transgressive  
478 features known as potholes may be induced by extension of the subsiding cumulate pile,  
479 particularly the larger examples. Magmatic erosion of the side walls may modify the shapes  
480 of these potholes.

481 Many questions remain to be solved. For example, the proposed model is likely not  
482 applicable to all transgressive features, namely small sub-circular dimples described from the  
483 base of the UG2 chromitite at Karee mine (van der Merwe and Cawthorn, 2004) and  
484 elsewhere, which may have formed through thermal erosion (Campbell, 1986). Another  
485 unresolved issue is whether potholes are more common in the Bushveld Complex than in  
486 other layered intrusion, mainly because of limited exposure in the latter. The relatively larger  
487 size of the Bushveld Complex could have resulted in enhanced crustal subsidence and slower  
488 cooling, favouring mobilisation of erosive crystal slurries. A further factor could be the  
489 presence of the Transvaal dolomite platform below the Bushveld. If this released substantial  
490 CO<sub>2</sub> to the Bushveld magma chamber during contact metamorphism, the resulting bubbles  
491 could have resulted in significant reduction of magma viscosity (Leshner and Spera, 2012),  
492 facilitating cumulate mobilisation and footwall erosion.

493

## 494 **9. Acknowledgements**

495 We thank African Thunder Platinum and Smokey Hills Mine for access to their property and  
496 samples, in particular chief mine geologist Paul Herron who spent a day guiding us around  
497 the exposures. Tony Oldroyd is thanked for producing the thin sections. Constructive reviews  
498 were provided by two anonymous reviewers.

499

## 500 **References**

501 Arndt, N.T., 2013. The formation of massif anorthosite: Petrology in reverse, *Geoscience*  
502 *Frontiers* 4, 195–198.

503 Ashwal, L.D., 1990. *Anorthosites*, Springer Verlag, Berlin, 422pp.

- 504 Barnes, S-J, Maier, W.D., Curl, E., 2010. Composition of the marginal rocks and sills of the  
505 Rustenburg Layered Suite, Bushveld Complex, South Africa: Implications for the formation  
506 of the PGE deposits. *Economic Geology* 105, 1491-1511.
- 507 Boorman, S.L., McGuire, J.B., Boudreau, A.E., Kruger, F.J., 2003. Fluid overpressure in  
508 layered intrusions: formation of a breccia pipe in the eastern Bushveld Complex, Republic of  
509 South Africa. *Mineralium Deposita* 38, 356-369.
- 510 Boudreau, A.E., 1988. Investigations of the Stillwater Complex IV. The role of volatiles in  
511 the petrogenesis of the J-M Reef, Minneapolis adit section. *Canadian Mineralogist* 26, 193–  
512 208.
- 513 Campbell, I.H. , 1986. A fluid dynamic model for the potholes of the Merensky Reef. *Econ*  
514 *Geol.*, 81, 1118-1125.
- 515 Czamanske, G. K., Bohlen, S. R. 1990. The Stillwater Complex and its anorthosites: an  
516 accident of magmatic underplating? *American Mineralogist* 75, 37-45.
- 517 Eales, H.V., Marsh, J.S., Mitchell, A.A., De Klerk, W.J., Kruger, F.J., Field, M., 1986. Some  
518 geochemical constraints upon models for the crystallization of the Upper Critical Zone-Main  
519 Zone interval, northwestern Bushveld Complex. *Mineralogical Magazine* 50, 567-582.
- 520 Eales, H.V., Field, M., de Klerk, W.J., Scoon, R.N., 1988. Regional trends of chemical  
521 variation and thermal erosion in the Upper Critical Zone, western Bushveld Complex.  
522 *Mineralogical Magazine* 52, 63-79.
- 523 Eales, H.V., De Klerk, W.J., Teigler, B., 1990. Evidence for magma mixing processes within  
524 the Critical and Lower Zones of the northwestern Bushveld Complex, South Africa.,  
525 *Chemical Geology* 88, 261-278.
- 526 Forien, M., Tremblay, J., Barnes, S.-J., Burgisser, A., Page, P., 2016. The Role of Viscous  
527 Particle Segregation in forming Chromite Layers from Slumped Crystal Slurries: Insights  
528 from Analogue Experiments. *Journal of Petrology*, doi: 10.1093/petrology/egv060
- 529 Gain, S.B., 1985. The geologic setting of the platiniferous UG2 chromitite layer on  
530 Maandagshoek, eastern Bushveld Complex. *Economic Geology* 80, 925-943.
- 531 Hess, H.H., 1960. Stillwater igneous complex. *Memoir of the Geological Society of America*  
532 80, 1-230.

- 533 Irvine, T.N., Andersen, J.C.O., Brooks, C.K., 1998. Included blocks (and blocks within  
534 blocks) in the Skaergaard Intrusion: Geological relations and the origins of rhythmic modally  
535 graded layers. *Bulletin of the Geological Society of America* 110, 1398-1447.
- 536 Kushiro, I., 1980. Viscosity, density, and structure of silicate melts at high pressures and their  
537 petrological applications. In: Hargraves, R.B. (Ed.), *Physics of Magmatic Processes*.  
538 Princeton University Press, Princeton, pp. 93–120.
- 539 Leshner, C.E., Spera, F.J., 2015. Thermodynamic and transport properties of silicate melts and  
540 magma. 113-141, In H Sigurdsson, B Houghton, S McNutt, H Rymer, J Stix (Eds), *The*  
541 *Encyclopedia of volcanoes*, Academic Press, 1422 pp.
- 542 Maaloe, S. 1978. The origin of rhythmic layering. *Mineralogical Magazine* 42, 337-345.
- 543 Morse, S.A., 1979a. Kiglapait geochemistry I: Systematics, sampling, and density. *Journal of*  
544 *Petrology* 20, 555-590.
- 545 Morse, S.A., 1979b. Kiglapait geochemistry II: Petrography. *Journal of Petrology* 20, 591-  
546 624.
- 547 Morse, S.A., 1986. Convection in aid of adcumulus growth. *Journal of Petrology* 27, 1183-  
548 1214.
- 549 Maier, W.D., 1995. Olivine oikocrysts in Bushveld anorthosite: some implications for  
550 cumulate formation: *Canadian Mineralogist* 33, 1011-1022.
- 551 Maier, W.D., Eales, H.V., 1997. Correlation within the UG2 - Merensky Reef interval of the  
552 Western Bushveld Complex, based on geochemical, mineralogical and petrological data:  
553 *Geological Survey of South Africa, Bulletin* 120, 56 pp.
- 554 Maier, W.D., Barnes, S-J., 2008. Platinum-group elements in the UG1 and UG2 chromitites  
555 and the Bastard reef at Impala platinum mine, western Bushveld Complex, *South African*  
556 *Journal of Geology* 111, 159-176.
- 557 Maier, W.D., Rasmussen, B., Li, C., Barnes, S-J., Huhma, H., 2013. The Kunene anorthosite  
558 complex, Namibia, and its satellite bodies: geochemistry, geochronology and economic  
559 potential. *Economic Geology* 108, 953–986.
- 560 Maier, W.D., Barnes, S-J, Groves, D.I., 2013. The Bushveld Complex, South Africa:  
561 Formation of platinum-palladium, chrome and vanadium- rich layers via hydrodynamic

- 562 sorting of a mobilized cumulate slurry in a large, relatively slowly cooling, subsiding magma  
563 chamber. *Mineralium Deposita* 48, 1-56.
- 564 Merensky, H., 1926. Die neuentdeckten Platinfelder im mittleren Transvaal, und ihre  
565 wissenschaftliche Bedeutung. *Berliner Zeitschrift der Deutschen Geologischen Gesellschaft*  
566 78, 298-314.
- 567 Mondal, S.K., Mathez, E.A., 2007. Origin of the UG2 chromitite layer, Bushveld Complex.  
568 *Journal of Petrology* 48, 495-510.
- 569 Mossom, R. J. 1986. The Atok platinum mine. In: Anhaeusser, C.R., Maske, S. (Eds.),  
570 Mineral deposits of Southern Africa. Geological Society of South Africa, Johannesburg, pp  
571 1143-1154.
- 572 Naldrett, A.J., Gasparri, E.C., Barnes, S.J., Von Gruenewaldt, G., Sharpe, M.R., 1986. The  
573 Upper Critical Zone of the Bushveld Complex and the origin of Merensky-type ores.  
574 *Economic Geology* 81, 1105-1117.
- 575 Naldrett, A.J., Wilson, A., Kinnaird, J., Yudovskaya, M., Chunnett, G., 2011. The origin of  
576 chromitites and related PGE mineralization in the Bushveld Complex: new mineralogical and  
577 petrological constraints. *Mineralium Deposita* 47, 209-232.
- 578 Naslund, H.R., McBirney, A.R., 1996. Mechanisms of formation of igneous layering. In:  
579 Cawthorn, R.G., (Ed.), *Layered intrusions*, Elsevier, Amsterdam, pp. 1-43.
- 580 Nicholson, D.M., Mathez, E.A., 1991. Petrogenesis of the Merensky Reef in the Rustenburg  
581 section of the Bushveld Complex. *Contributions to Mineralogy and Petrology* 107, 293-309.
- 582 O'Driscoll, B., Donaldson, C.H., Daly, J.S., Emeleus, C.H. 2009. The roles of melt  
583 infiltration and cumulate assimilation in the formation of anorthosite and a Cr-spinel seam in  
584 the Rum Eastern Layered Intrusion. *Lithos* 111, 6–20.
- 585 Paterson, S.R., 2009. Magmatic tubes, pipes, troughs, diapirs, and plumes: Late-stage  
586 convective instabilities resulting in compositional diversity and permeable networks in  
587 crystal-rich magmas of the Tuolumne batholith, Sierra Nevada, California. *Geosphere* 5, 496-  
588 527.
- 589 Scoates, J.S., Lindsley, D.H., Frost, B.R., 2010. Magmatic and structural evolution of an  
590 anorthositic magma chamber: The Poe Mountain intrusion, Laramie Anorthosite Complex,  
591 Wyoming. *Canadian Mineralogist* 48, 851-885.

592 Scoon, R.N., Mitchell, A.A., 1994. Discordant iron-rich ultramafic pegmatites in the  
593 Bushveld Complex and their relationship to iron-rich intercumulus and residual liquids.  
594 *Journal of Petrology* 35, 881-917.

595 Scoon, R.N., Mitchell, A.A., 2004. The platiniferous dunite pipes in the eastern limb of the  
596 Bushveld Complex: Review and comparison with unmineralized discordant ultramafic  
597 bodies. *South African Journal of Geology* 107, 505-520.

598 Tanner, D., Mavrogenes, J.A., Arculus, R.J., Jenner, F.E., 2014. Trace Element Stratigraphy  
599 of the Bellevue Core, Northern Bushveld: Multiple Magma Injections obscured by diffusive  
600 processes. *Journal of Petrology* 55,859-882.

601 Van der Merwe, J., Cawthorn, R.G., 2005. Structures at the base of the Upper Group 2  
602 chromitite layer, Bushveld Complex, South Africa, on Karee Mine (Lonmin Platinum),  
603 *Lithos* 83, 214-228.

604 Wallace, P.J., Plank, T., Edmonds, M., Hauri, E.H., 2015. Volatiles in magmas, 163-183. In  
605 H Sigurdsson, B Houghton, S McNutt, H Rymer, J Stix (Eds), *The Encyclopedia of*  
606 *volcanoes*, Academic Press, 1422 pp.

607

## 608 **Figure Captions**

609 Figure 1: (A) Simplified geological map of the Bushveld Complex. (B) Geological map of  
610 the farm Maandagshoek, showing location of studied exposures (star symbol). (C)  
611 Stratigraphic column, with average thicknesses of layers (modified from African Thunder  
612 unpublished report). Peg Px = pegmatoidal pyroxenite; MN = melanorite; MGb =  
613 melagabbro; An = anorthosite; No = norite; Cr = chromitite.

614 Figure 2: Large anorthosite pothole at Smokey Hills mine. View from NE, with key features  
615 discussed in the text indicated.

616 Figure 3. The UG2 chromitite as exposed along the access road to Smokey Hills mine. (A)  
617 Note thin elongated pyroxenite autolith in upper portion of seam, and sharp, but undulating  
618 bottom contact. Inset shows lens-like pegmatoidal rock with chromitite selvage within the  
619 UG2 seam, representing either an autolith or an intrusion. (B) The UG2 seam is split by a  
620 large autolith of pyroxenite, locally resulting in slight updoming of the upper contact of the



621 seam. Also note a band of anorthosite-pyroxenite near basal contact (arrow), and pods of  
622 anorthosite associated with the leader seams (arrow at upper right).

623 Figure 4: The UG2 hanging wall marker layers consist of 2 anorthosite seams within a 1 m  
624 interval of banded norite. Note cusps and flames of anorthosite extending into the hanging  
625 wall norite, and several thin schlieren and lenses of anorthosite between the marker layers.  
626 (A) Overview of layered interval hosting the marker layers, (B) close-up of highlighted area  
627 from (A), with arrow pointing to small pothole of anorthosite in norite. (C+D) Further  
628 examples of anorthosite flames or cusps extending into banded hanging wall norite.

629 Figure 5: Rocks from the sequence between the UG2 hanging wall marker layers and the  
630 UG3 chromitite. (A) UG3 chromitite, underlain by anorthosite footwall, magmatic breccia of  
631 melanorite fragments containing anorthosite fragments within leuconoritic matrix (yellow  
632 arrow), and banded norite. (B) Banded norite containing blocky anorthosite autoliths below  
633 UG3 chromitite. (C) The UG3 footwall anorthosite seemingly injects its footwall and hanging  
634 wall. Note that anorthosite consists of upper mottled portion, central weakly banded portion,  
635 and lower schlieren-banded portion. (D) Melanorite lenses within UG3 footwall anorthosite.

636 Figure 6: (A) Large mass of intrusive anorthosite occurring in thinned pyroxenite-chromitite  
637 sequence of southern pit. Thinning of sequence is reflected by downwarping of UG3a+b  
638 seams. (B) Close-up of UG3 chromitite invaded by pyroxenite. (C) Fragmentation of UG3  
639 chromitite by intruding anorthosite.

640 Figure 7: (A) The contact between the MR footwall 8 anorthosite and the UG3 hanging wall  
641 pyroxenite / melanorite. Note autoliths of banded melanorite on left and right (yellow  
642 arrows), and several intrusions of IRUP. (B) Trough banding (yellow stippled lines) in  
643 anorthosite within large pothole of Fig. 2. (C) Transgressive irregular contact between  
644 melanorite and anorthosite on southern sidewall of large anorthosite pothole. Note sideway  
645 extension of melanorite into the pothole (red arrow). Also note pinching out of UG3 as  
646 pothole edge is approached. (D) Contact chromitite stringer between UG3b HW pyroxenite  
647 and MR FW8 anorthosite. (E) Textural variability of MR FW8 mottled anorthosite. (f)  
648 Melanorite of UG3b hanging wall.

649 Figure 8: Relationships between anorthosite pothole and its sidewall. (A) Dislodgement of  
650 pyroxenite and chromitite by intruding anorthosite. (B) Intrusion of anorthosite above and  
651 below UG3 chromitite. (C) Relationships in northern portion of pothole. Note change in dip  
652 below pothole (lower yellow arrow) interpreted to result from flexure prior to pothole

653 formation, coincident with location of intrusive anorthosite lens (upper yellow arrow). Also  
654 note how anorthosite magma carves out the sidewall at the contact between lithologies. (D)  
655 Close-up of anorthosite lens from (C). The anorthosite forms pegmatoidal upward extensions  
656 into the norite and it contains lenses of what appears to be pegmatoidal pyroxenite, possibly  
657 IRUP.

658 Figure 9: Photomicrographs of analysed rocks. (A) Anorthosite, sample 1. (B) Norite, sample  
659 1. (C) Anorthosite, sample 2. (D) Norite, sample 2. (E) Anorthosite, sample 3. (F)  
660 Anorthosite, sample 4.

661 Figure 10: Element map of sample 1, showing strings of plagioclase and orthopyroxene  
662 within melanorite.

663 Figure 11: Schematic model of formation of anorthosite pothole on Smokey Hills. See text  
664 for further explanation.

665

666

667 Figure 12: Sketch model of pothole formation in Bushveld Complex. In steps 1–3 layering  
668 forms due to subsidence and sorting of noritic proto cumulates. In steps 4–6, flexing of the  
669 cumulate sequence results in pull apart structures into which anorthosite slurries plunge. Also  
670 note injection of anorthosite into semi solidified cumulus sequence, notably in areas of  
671 enhanced stretching.

672

### 673 **Electronic Appendices**

674 ElectronicAppendix 1: Banded anorthosite-norite of sample 2. Note distinct foliation in  
675 anorthosite, expressed in the form of mm-wide bands of anorthosite and leuconorite.

676 Electronic Appendix 2: Element map across a norite band within anorthosite of sample 2.  
677 Note pervasive reversed zoning in plagioclase, and lack of compositional variation between  
678 anorthosite and norite.

679 Electronic Appendix 3: Zoning in cumulus plagioclase of the UG2-Merensky Reef interval,  
680 western Bushveld Complex

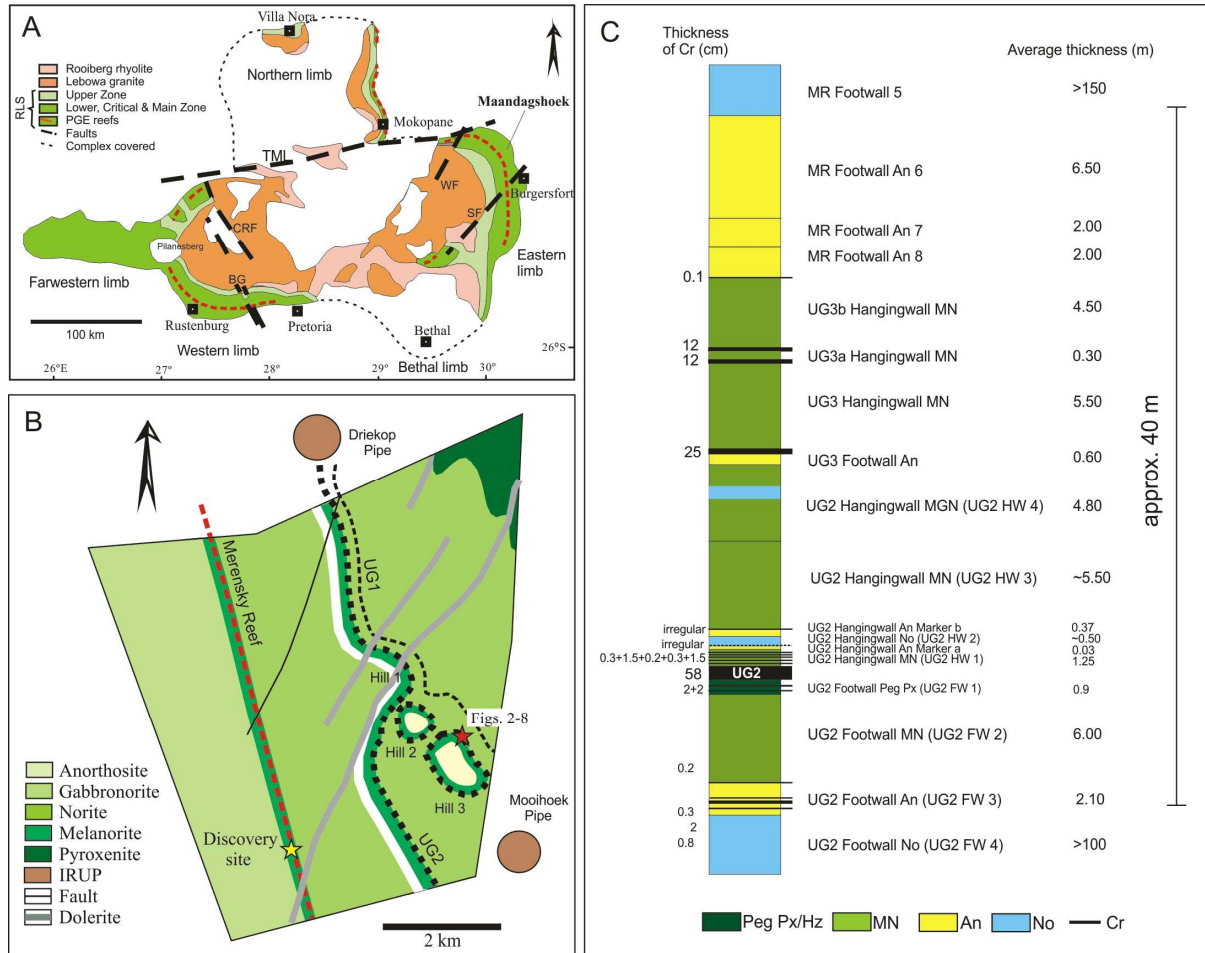
681 Electronic Appendix 4: Mineral compositions in samples 1 and 2 (SH1 and 2)

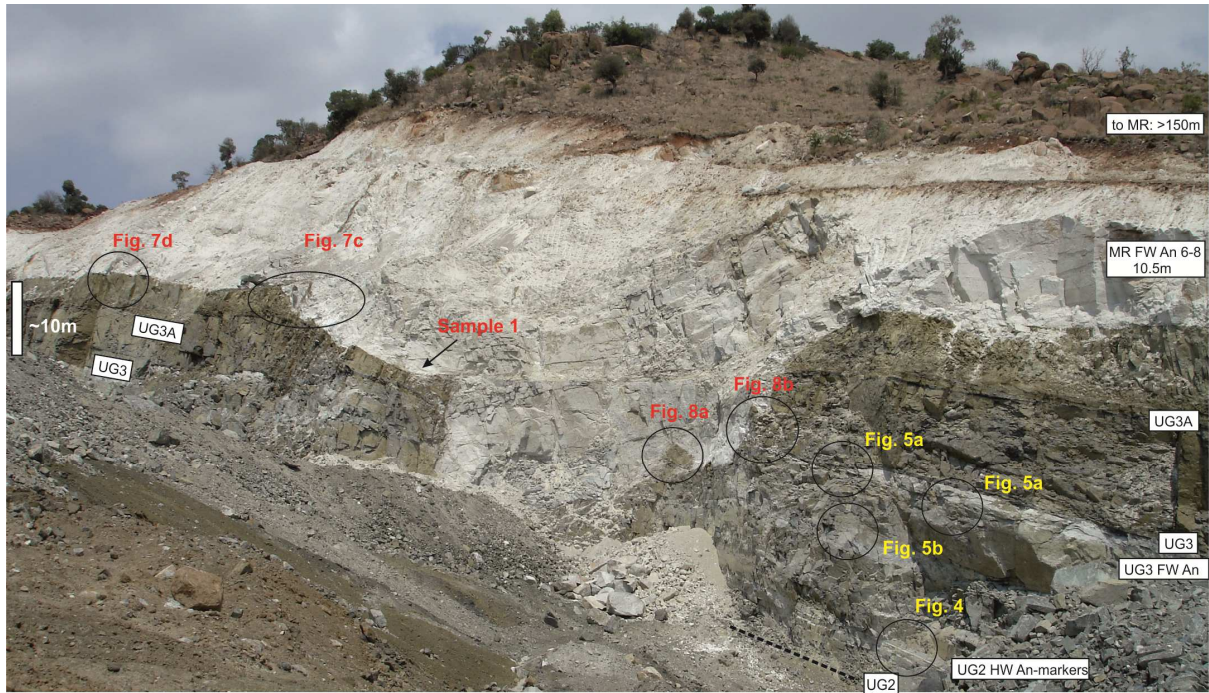
682 Electronic

683 Appendix 5: Breccia pipe of anorthosite-norite fragments within iron-rich ultramafic matrix

684 at Tweefontein, eastern Bushveld Complex. Contacts of pipe are delineated by persons

685 (photograph courtesy of Richard Arculus).

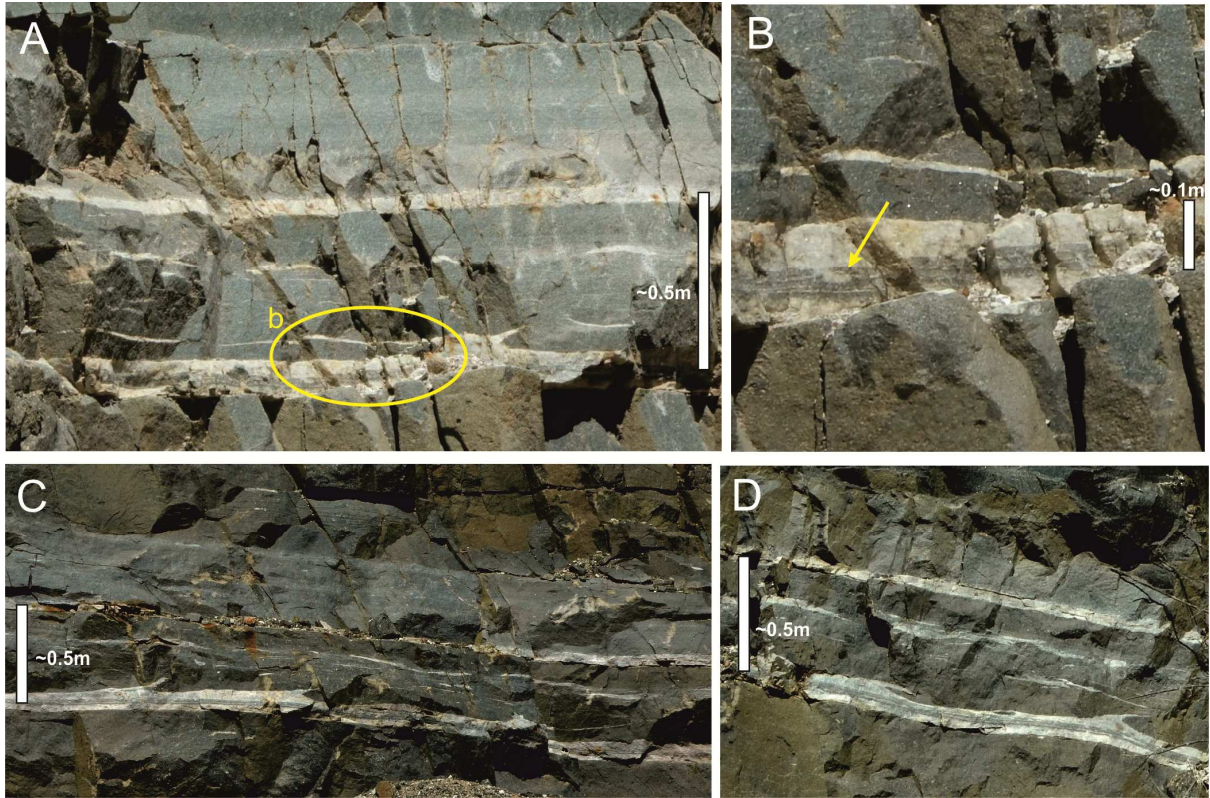


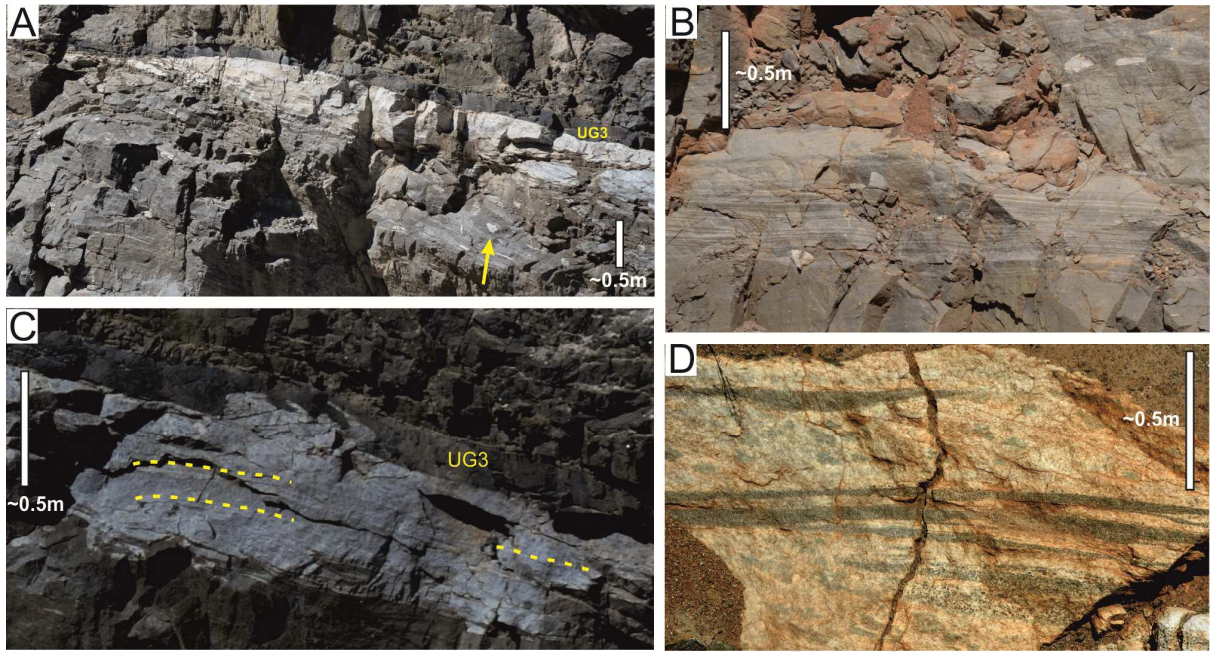




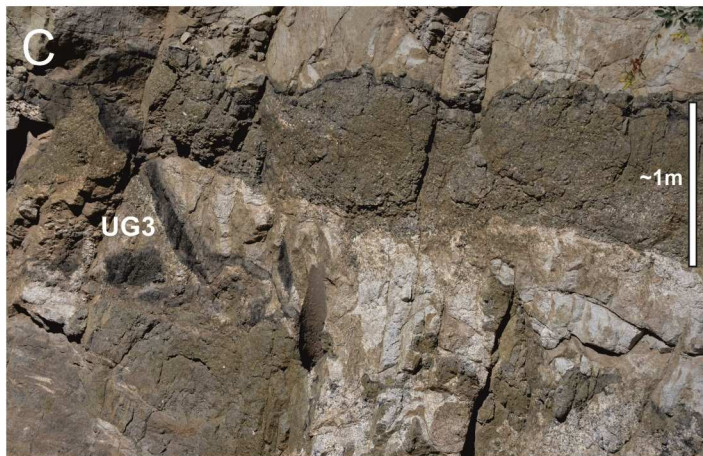
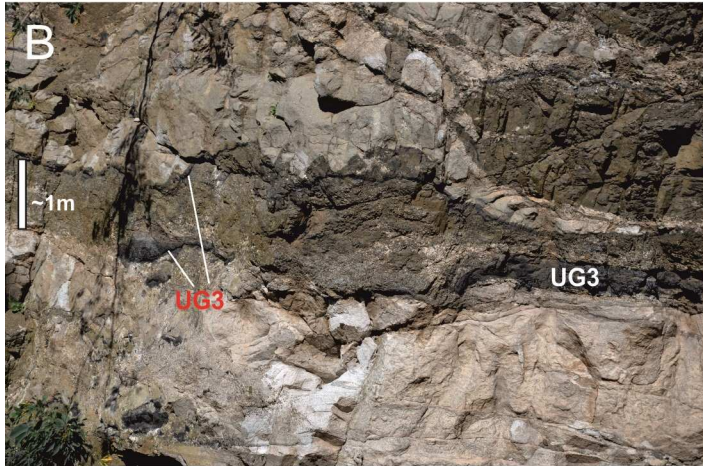
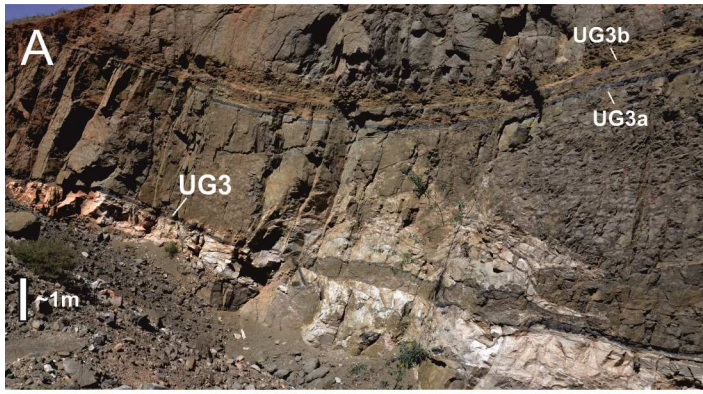


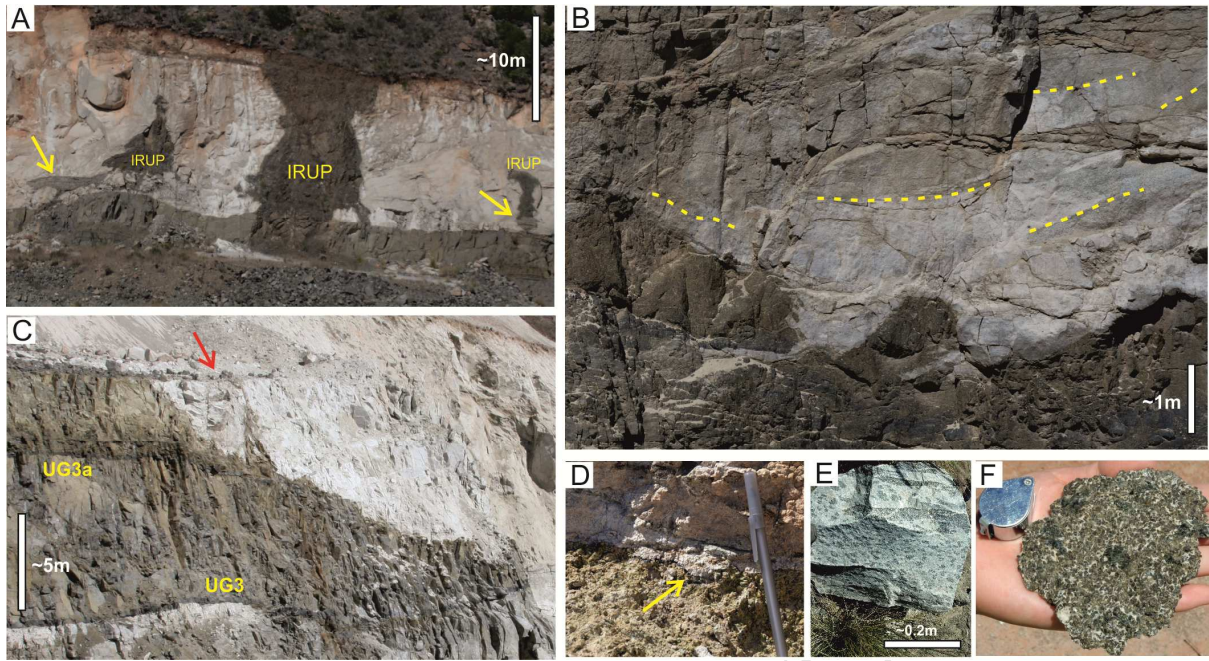




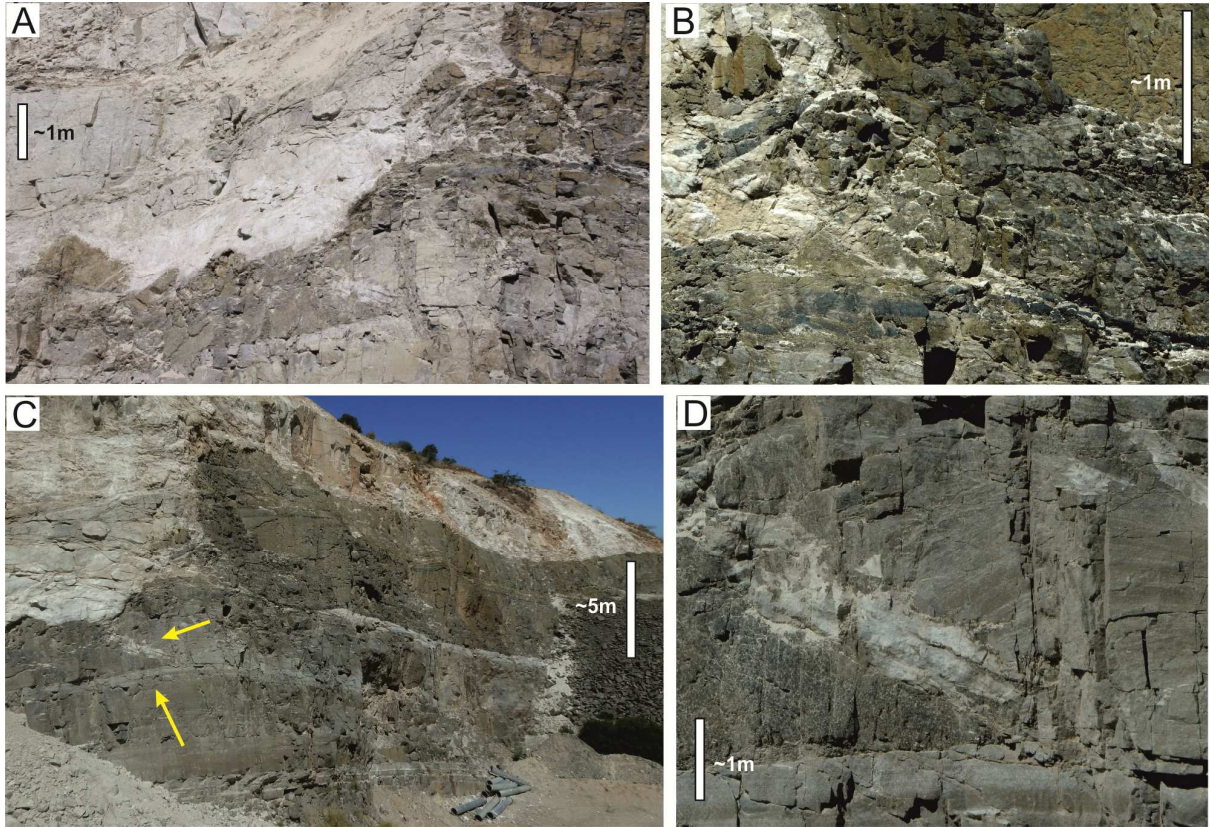




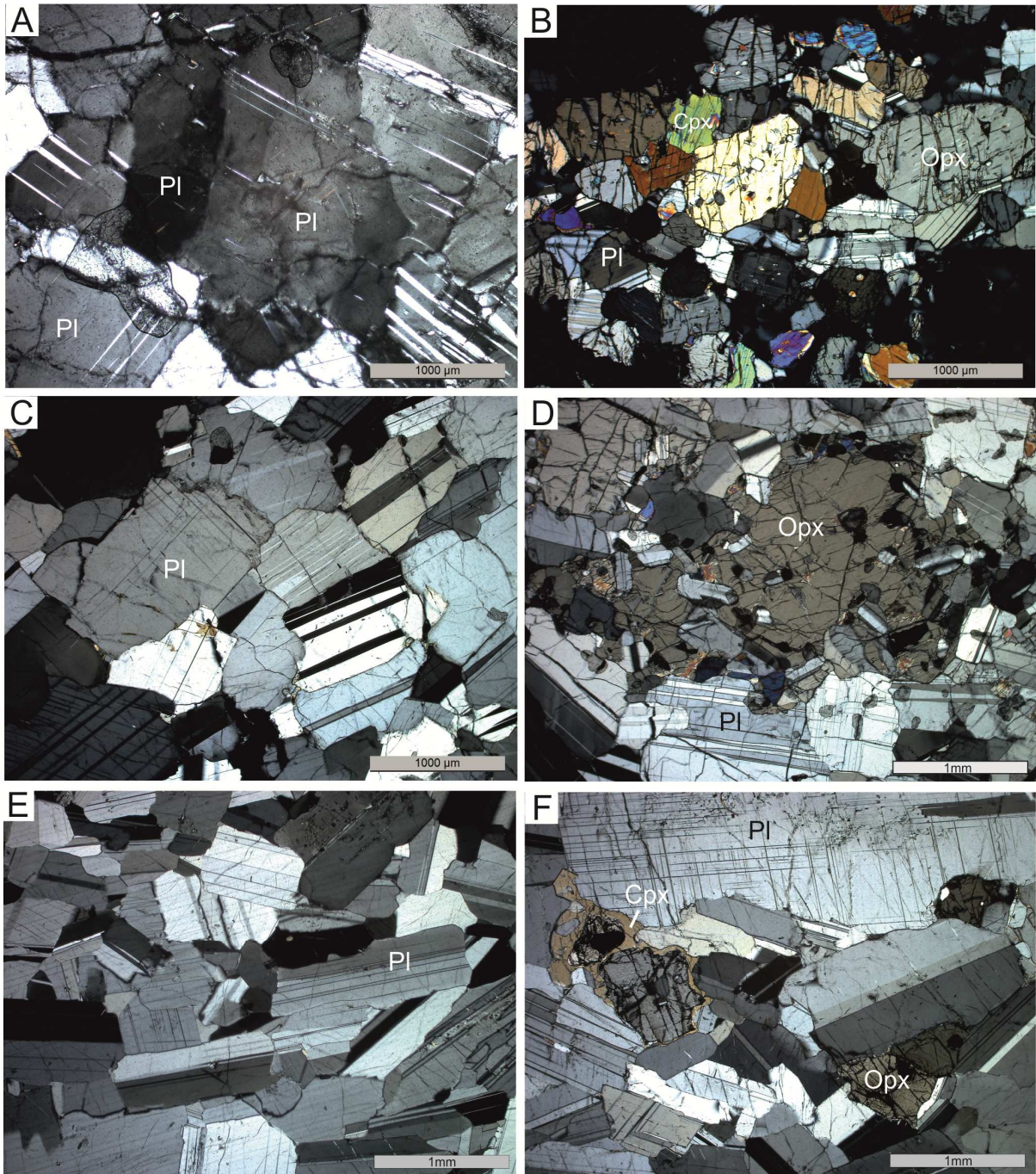




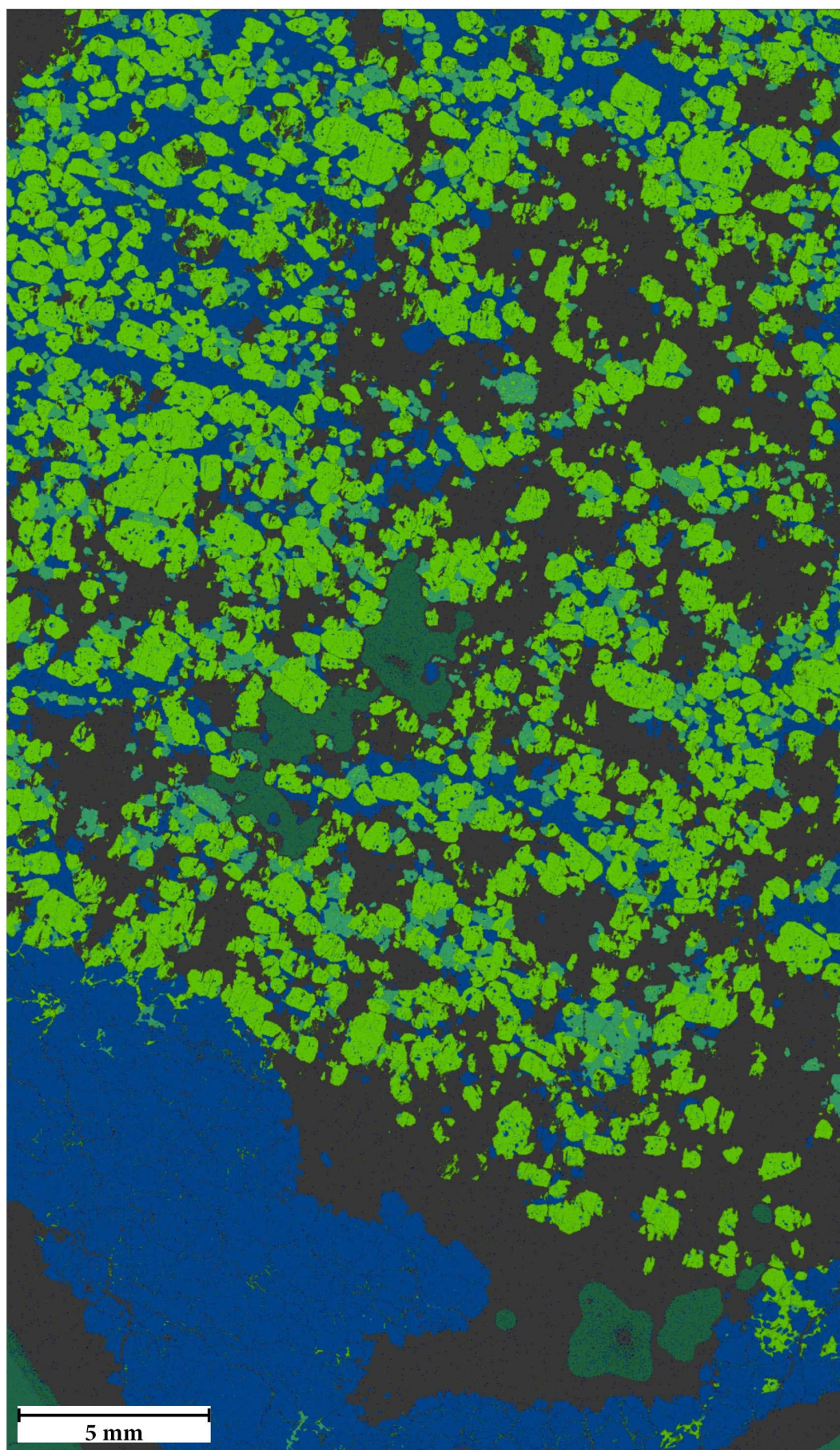








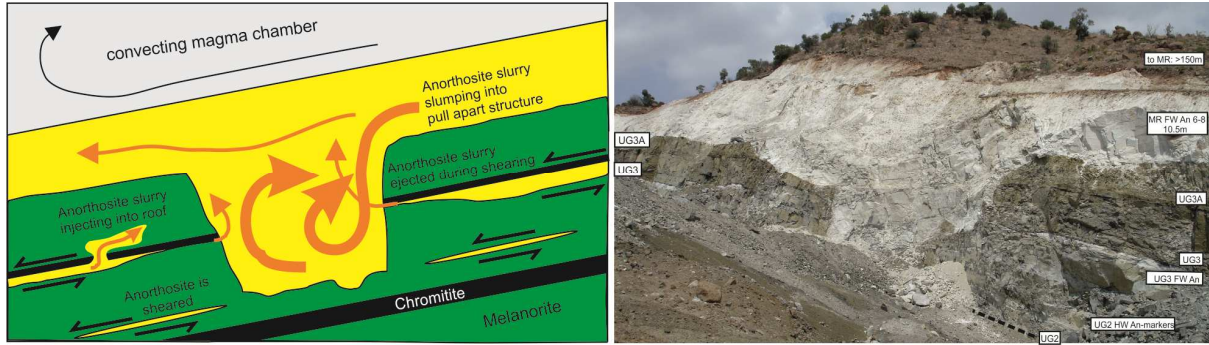




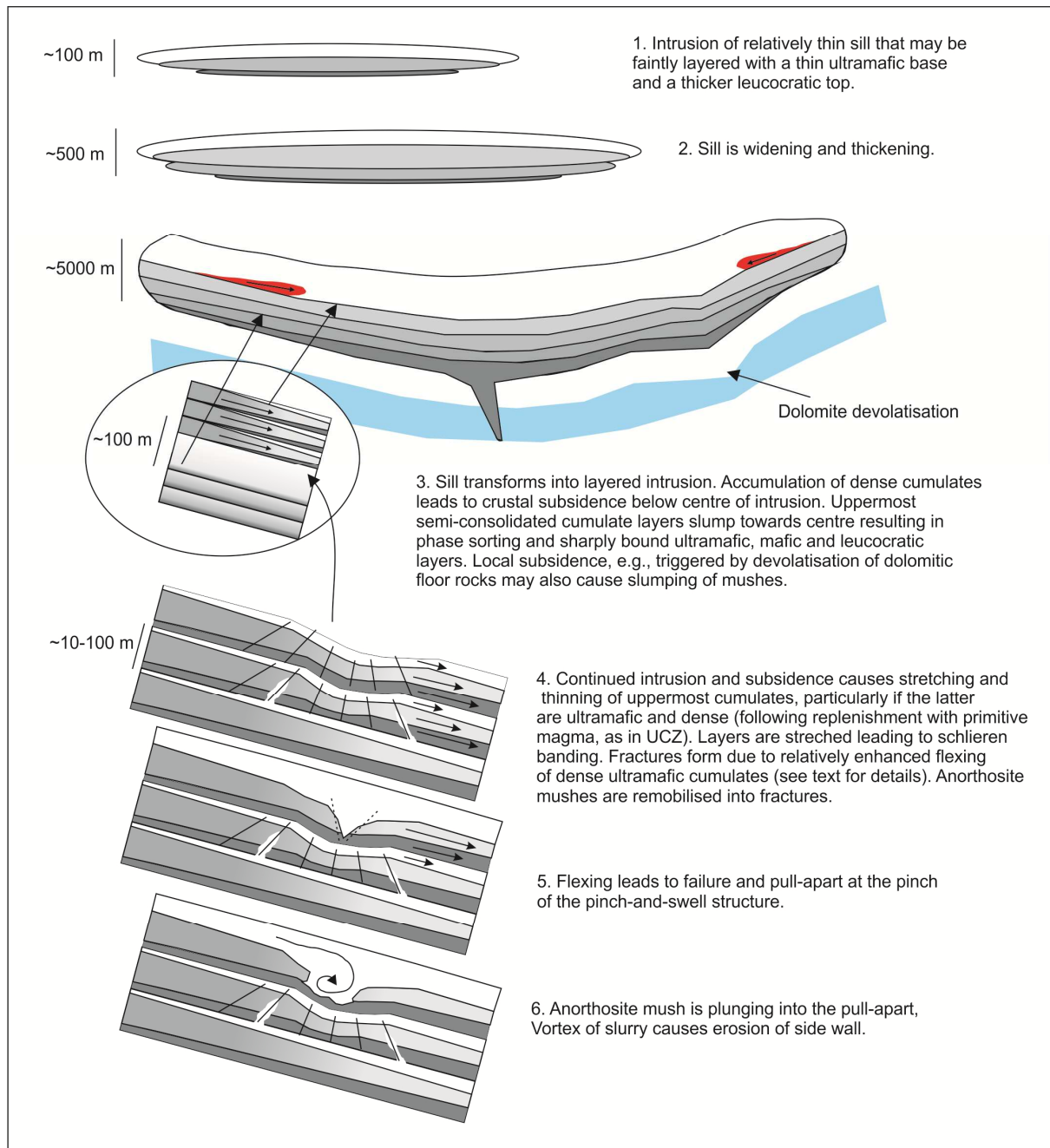
■ Plagioclase

■ Orthopyroxene

■ Clinopyroxene







**Highlights**

- Anorthosites act as lubrication planes during tectonism of layered intrusions
- Mobilised plagioclase-rich slurries may form intrusive anorthosites
- Anorthositic adcumulates form through down-dip draining of Fe rich residual liquid